Impact of upstream runoff and tidal level on the chlorinity of an estuary in a river network: a case study of Modaomen estuary in the Pearl River Delta, China

Yanhu He, Sha Chen, Ruizhen Huang, Xiaohong Chen and Peitong Cong

ABSTRACT

Saltwater intrusion exerts great impact on water supply and water withdrawal from estuarine areas. A chlorinity prediction model based on backpropagation neural network was constructed, calibrated, and validated, considering phase lags, with the Modaomen estuary in the Pearl River Delta (PRD), China as case study. This study aimed to investigate impacts of upstream runoff and tidal level on the changing properties of estuarine chlorinity. Nine boundary conditions – low tide and tidal range both with three different frequencies – were designed to explore the changing process of estuarine chlorinity and obtain the critical upstream runoff for saltwater suppression. Results indicated the model performed efficiently; Nash–Sutcliffe efficiency coefficient and R^2 were both 0.91 in training period, 0.76 and 0.82 in testing period, and 0.64 and 0.77 in validation period, respectively, and estuarine chlorinity shows slightly different changing processes of decline rate under the nine boundary conditions when the upstream runoff increases. The higher the designed tidal range and lower daily tides together with the smaller the amount of upstream runoff, the higher the estuarine chlorinity. The critical upstream runoff of the Pinggang pumping station is 2,500 m^3/s. These findings provide a foundation for water supply security and upstream reservoir dispatching in estuarine areas in dry periods.

Key words | backpropagation neural network, chlorinity, Modaomen estuary, saltwater intrusion, upstream reservoir dispatching

Yanhu He
Sha Chen
Ruizhen Huang
Xiaohong Chen (corresponding author)
Center for Water Resources and Environment,
Sun Yat-sen University,
Guangzhou 510275,
China
and
Guangdong Engineering Technology Research Center of Water Security Regulation and Control for Southern China,
Sun Yat-sen University,
Guangzhou 510275,
China
E-mail: *eescxh@mail.sysu.edu.cn*

Ruizhen Huang
Water Conservancy Institute of Torch High-tech Industrial Development Zone in Zhongshan City,
Zhongshan 528437,
China

Yanhu He
Peitong Cong
College of Water Conservancy and Civil Engineering,
South China Agricultural University,
Guangzhou 510642,
China

INTRODUCTION

Located in the transition zone between the ocean and the river and subject to the forces of both the ocean and the river, an estuary typically provides convenient transportation and important habitats for human life and trade activities. Saltwater intrusion tends to significantly influence the ecosystem and water use in estuaries. Many factors affect saltwater intrusion (Liu *et al.* 2014), among which, upstream runoff and ocean tides are considered more important (Shaha *et al.* 2013; Yoon & Woo 2013; Lian *et al.* 2015). An increase in sea level due to an increase in temperature causes high tides in estuaries and aggravates the severity of saltwater intrusion (Ketabchi *et al.* 2016). Saltwater intrusion in estuaries leads to not only the deterioration of groundwater quality but also to soil salinization, which is potentially harmful to the use of groundwater and its surrounding agricultural production (Colon-Rivera *et al.* 2014; Vijay & Mohapatra 2016). Moreover, terrestrial freshwater resources are seriously affected because of increased water salinity and deterioration of water quality (Cheng *et al.* 2012; Liu *et al.* 2018); these resources also considerably impact tidal freshwater forested wetlands, in addition to saltwater (Colon-Rivera *et al.* 2014). Thus, it is important to

doi: 10.2166/hydro.2018.210

identify the characteristics of saltwater intrusion in estuaries and quantitatively evaluate the impact of upstream runoff on the chlorinity of the estuary.

Several studies on saltwater intrusion in estuaries have been conducted. For example, an analytical 1-D salt intrusion model was tested and shown to perform well in Shatt al-Arab River (Abdullah *et al.* 2016, 2018) and Malaysian estuaries (Gisen *et al.* 2015), compared with extensively observed data. Ongoing eutrophication and planned surface water withdrawals could drive saltwater intrusion in a Florida estuary (Williams *et al.* 2014). The impact of reductions in freshwater flow to the Richmond River estuary in Australia on saltwater intrusion was assessed based on hydrological and freshwater extraction data (Peirson *et al.* 2001). In China, multi-dimensional numerical models were developed to forecast the salinity of river estuaries in response to the pattern of saltwater intrusion (Lian *et al.* 2015) and to investigate the influences of water conservancy projects, such as water diversion from the south to the north project and the Three Gorges Project, on saltwater intrusion in the Yangtze River estuary (An *et al.* 2009; Xu *et al.* 2012).

Owing to its combination of superior natural conditions and abundant resources, the Pearl River Delta (PRD), one of the three important economic center regions in China, is densely populated, with concentrated industry and rapid development. The PRD is also one of the most threatened estuaries in the world, as it has been exposed to an increasing series of crises related to water resources. Water conflict, water pollution, and saltwater intrusion have all increased dramatically in the past few decades, and pose a threat to regional water security and impose constraints on regional development. Regarding the estuary in the PRD (He *et al.* 2016), the abrupt change in topography and the rise in sea level (Zhang *et al.* 2013) have been considered crucial factors causing saltwater intrusion outbreaks in estuaries. Apart from the aforementioned examples, which illustrate how saltwater intrusion impacts estuaries, other models are also found in the literature. Previous studies provide a foundation for the changes in properties, causes, and implications of the chlorinity of estuaries, as well as long-term forecast of estuarine chlorinity. Multi-dimensional numerical models are used as effective tools to investigate the dynamic characteristics of saltwater intrusion and explore its impacts on water supply in estuaries. However, compared with the impact of a rise in sea level on the chlorinity of estuaries, studies on the compound effect of upstream runoff and tide level changes remain insufficient, but it is essential to obtain the critical upstream runoff for saltwater suppression and conduct real-time runoff regulation of upstream reservoir. In addition, the application of multi-dimensional numerical models would be restricted without observed chlorinity and hydrological data, as well as large-scale estuarine topography.

Estuary chlorinity is highly nonlinear and the spatial-temporal variability of estuary chlorinity requires the estimation procedure to be dynamic (Liu *et al.* 2014; Ketabchi *et al.* 2016). Such a dynamic relationship can be modeled carefully by artificial neural networks (ANNs), similarly to the application of ANNs in other hydrology simulation areas (Abrahart *et al.* 2008, 2012). As a data-driven model, an ANN model can be used to simulate and forecast the chlorinity of estuaries, due to its ability to capture the nonlinear relation of acquisition elements when sufficient hydrological, tidal, and chlorinity data are available and has good representativeness. Based on such an optimal data set that is representative of the probable occurrence of an input vector and can facilitate the mapping of the underlying nonlinear process, optimal weight matrices and bias vectors are found in an ANN model through a training process to generate reasonable results given new inputs (ASCE 2000).

The Modaomen waterway, an important estuary of the Pearl River, encountered the most severe salt intrusion in December 2011. Topography, spring–neap tidal variation, local wind stress, and their interactions are identified as the driving factors for the abnormal characteristic of saltwater intrusion in the Modaomen waterway (Wang *et al.* 2012). Moreover, the closure of Hongwan waterway and Hezhou waterway in the Modaomen estuary could decrease saltwater intrusion in the estuary (Gong *et al.* 2012). Salinity in the Modaomen waterway is largely affected by the tidal range during low-streamflow periods (Liu *et al.* 2014). Affected by the upstream runoff and tidal cycle, Modaomen waterway has had an excessive chlorinity since December 4, 2011. In particular, the Pinggang pumping station in Zhuhai City had an excessive chlorinity for 10 d continuously, which caused half-month periods of unavailable water withdrawals. Dredging campaigns have led to an abrupt change in

topography and an alteration in the flow split ratio between the North River and the West River, causing changes in both the tidal range and saltwater intrusion in the Pearl River estuary (Liu *et al.* 2010; Yuan & Zhu 2015). Given the above issues, in this case study of the Modaomen waterway, a chlorinity prediction model of the Pearl River estuary was constructed based on the backpropagation (BP) neural network and the performance efficiency of the model was evaluated. The chlorinity of the Pearl River estuary was simulated under different frequencies of upstream runoff and tide levels, and the compound effects of the changes in upstream runoff and tide levels on the changing properties of the Pearl River estuary chlorinity were investigated using the validated chlorinity prediction model.

The objectives of this study are as follows: (1) to build a chlorinity prediction model of the estuary based on BP neural networks and simulate the estuary chlorinity under different boundary conditions of upstream runoff and tide levels; (2) to explore the joint impacts of the changes in upstream runoff and tidal levels/range on the changing properties of the Pearl River estuary chlorinity and obtain the critical upstream runoff for saltwater suppression. The impact analysis can aid in gaining a better understanding of saltwater intrusion and drivers behind it in estuaries. Furthermore, the simulation results from the ANNs model can provide a foundation for the upstream reservoir dispatching according to the critical upstream runoff, aiming to control saltwater intrusion and alleviate its negative effect on water withdrawal, which will benefit water supply security of the estuaries challenged by sea level rise and extreme dry weather events. The remainder of this paper is organized as follows: The section below briefly describes the study area, associated data, and methodology, followed by a section that discusses and analyzes the results, and a final section that presents the major conclusions of the study.

MATERIALS AND METHODS

Study area

From the Pearl River estuary it is east to Shenzhen, west to Taishan, north to Guangzhou and south to Wanshan islands, including most parts of the PRD and the inner shelf waters. Its width is about 4 km at the northern end near Humen and about 60 km between Hong Kong and Macau at the southern end. The length between the two ends is about 63 km (Mao *et al.* 2004). The Modaomen estuary, a typical channel segment of the Pearl River estuary with active saltwater intrusion, is the main estuary of the West River (Figure 1). It is 33.35 km long and drains an area of 177.8 km^2. The annual sediment yield of the Modaomen estuary is 27 million t. Before 1999, saltwater intrusion mainly affected Tanzhou town in Zhongshan City; after 1999, saltwater intrusion became a more serious problem affecting urban and surrounding areas. The most severe salinity in the last 30 years occurred in 2005; the water supply to 18 of 24 towns in Zhongshan City was influenced by varying degrees of saltwater intrusion. In 2011, salinity downstream was extremely severe and Pinggang pumping station broke its chlorinity record of 2005.

Data

Tidal range (i.e., the difference between the adjacent high and low tide levels in a tidal cycle), spring–neap tidal variation, and upstream runoff were identified as the driving factors for the abnormal characteristic of saltwater intrusion in the Modaomen waterway in the Pearl River estuary (Wang *et al.* 2012; Liu *et al.* 2014; Yuan & Zhu 2015). Given this, in the current study, daily average runoff, low tide, and tidal range were chosen as the three input variables for proper mapping in the ANN model. Data used in this study consist of the average daily runoff (the summation of the average daily runoff of Sanshui and Makou stations), low daily tide (i.e., lowest of all tidal levels measured in a day), great diurnal range of Denglongshan station, and average daily chlorinity of the Pinggang pumping station, all of which were selected from the observed data for November 2015 to February 2016, and January 2007. The total number of samples is 150. Correlation analysis is used to analyze the correlation between the daily chlorinity of the i_{th} day and the same influencing factor, considering the phase lags between the average daily chlorinity and the affecting factors (e.g., daily runoff, low daily tide, and tidal range) (Liu *et al.* 2014). The correlations of the average daily chlorinity with each affecting factor under different phase lags were analyzed, and the affecting factor series

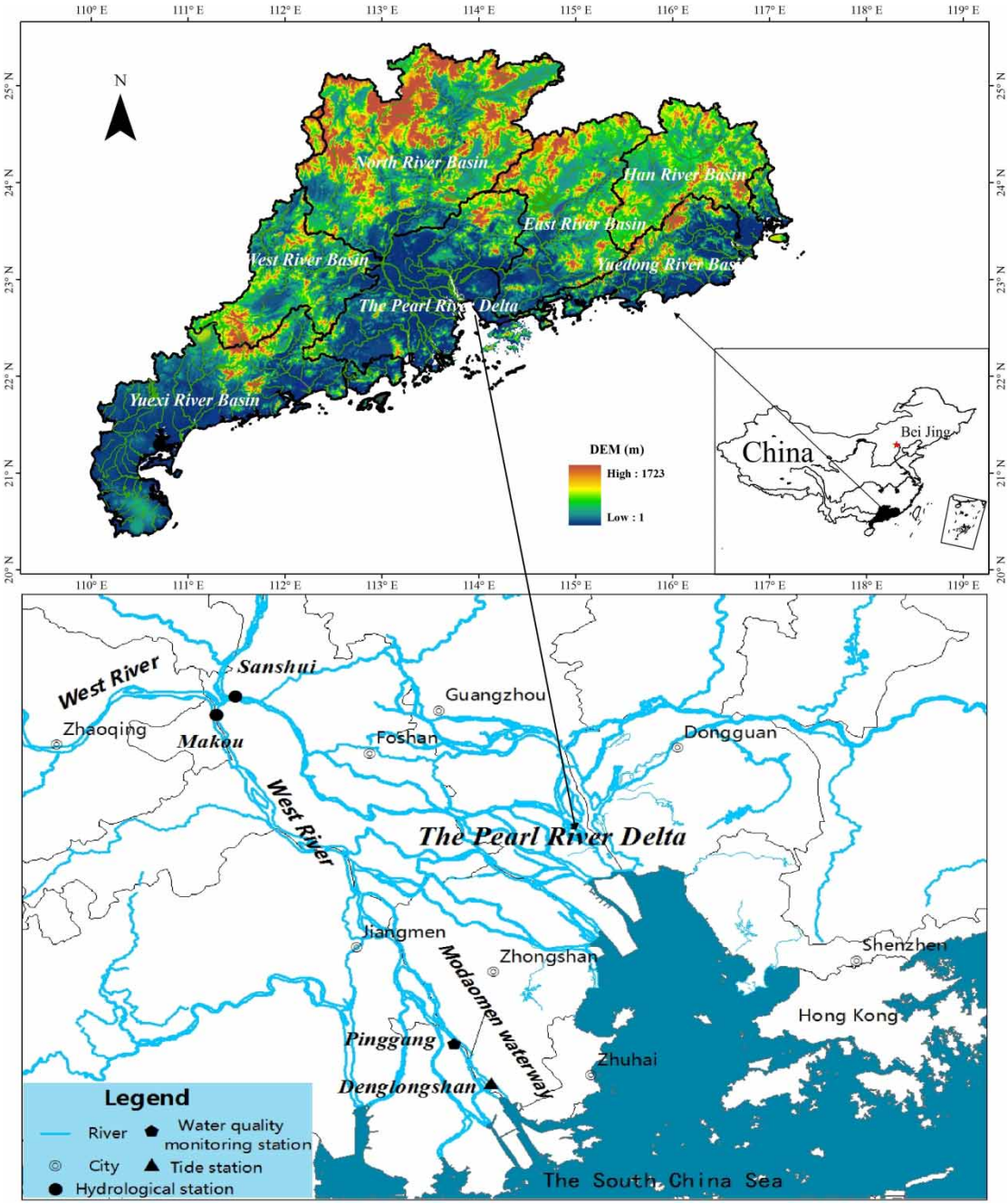

Figure 1 | Schematic of the Modaomen waterway.

that considered the phase lag with the highest correlation was chosen for the final input. The results show that there was the highest correlation between the daily chlorinity of the i_{th} day and the daily runoff of the $(i-2)_{th}$ day, and the low daily tide of the $(i+3)_{th}$ day and the tide range of the $(i+3)_{th}$ day. The available data are usually divided into training, testing, and validation subsets for an ANN model and a genetic algorithm (GA) was used to divide data into representative subsets (Bowden *et al.* 2005) in the current study. Therefore, data were divided into three groups and a total of 150 data records were considered as inputs for the ANN model development, from which 120 records

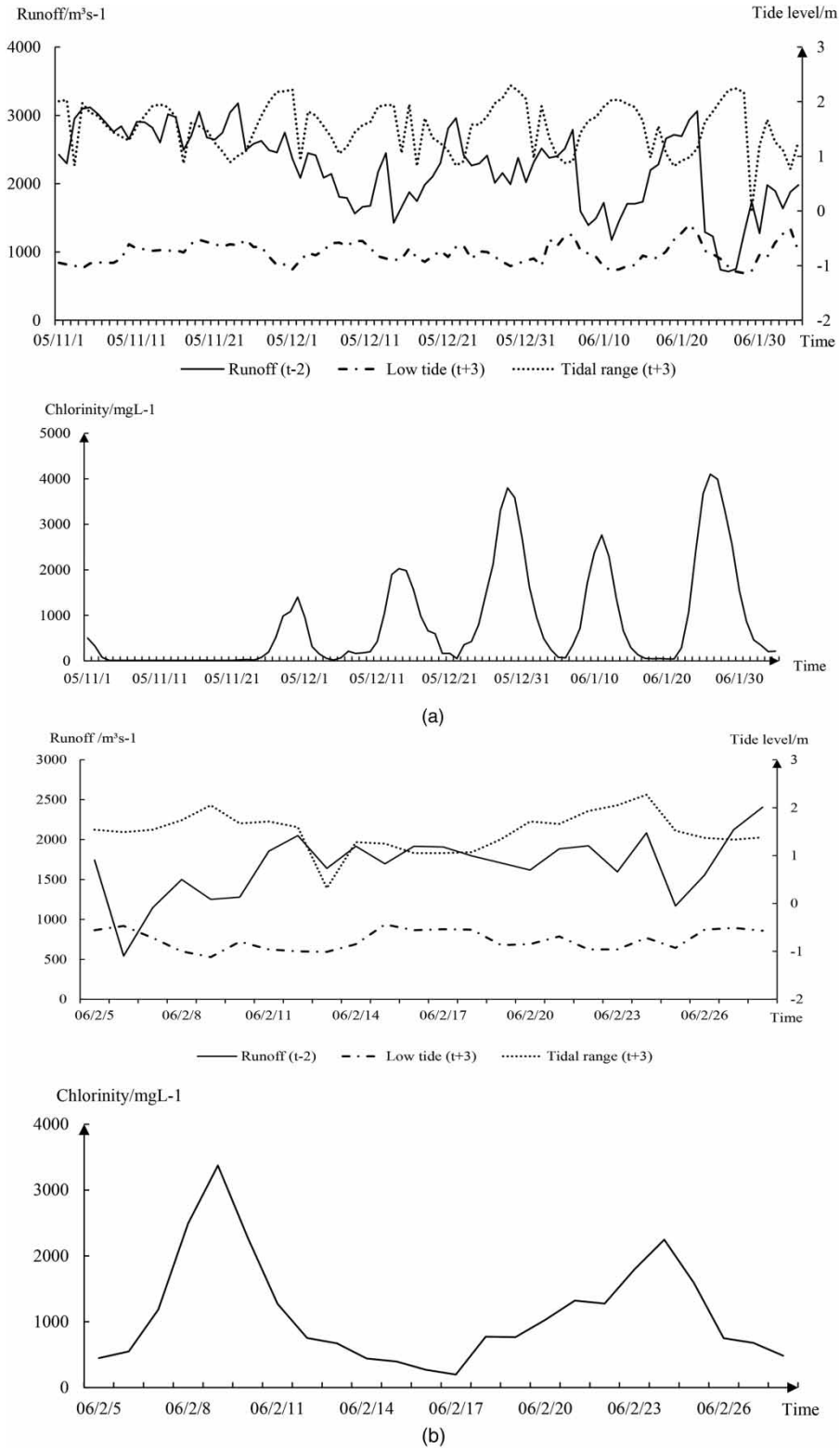

Figure 2 | Runoff, tide level, and chlorinity data for training (a), testing (b), and validation (c). *(Continued.)*.

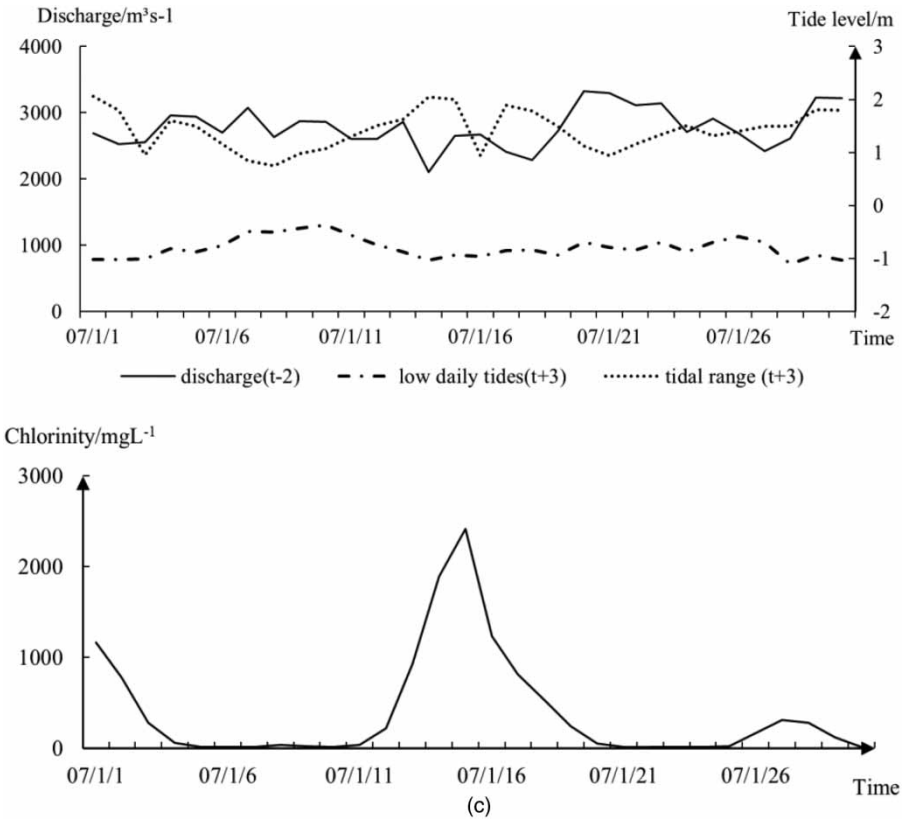

Figure 2 | Continued

(80%) were used for training and 30 records (20%) were used for validation (Figure 2(c)). The 120 records in the calibration set were further divided into 96 training records (80%) (Figure 2(a)) and 24 testing records (20%) (Figure 2(b)). The average daily runoff, as well as low tide and tidal range were the input data for the model, which were normalized with the premnmx function. Output data of the model include the average daily chlorinity at the Pinggang pumping station, and were anti-normalized with the postmnmx function after calibration and validation.

BP neural network

In recent years, ANNs have been widely applied in hydrological analysis and prediction, achieving satisfactory results. To obtain a complex mapping between input and output conditions, the structure for a multi-layer neural network is typically used. The BP ANN is the most widely used neural network model. Proposed by a team of scientists led by Rumelhart & McClelland (1987), the BP network is a multilayer feedforward network trained by the error BP algorithm. The three-layer network structure of the BP neural network (Figure 3) is the most commonly used structure to properly solve the hydrological research problem (Joshi *et al.* 2016). Thus, in the present study, the three-layer network structure was selected to establish the

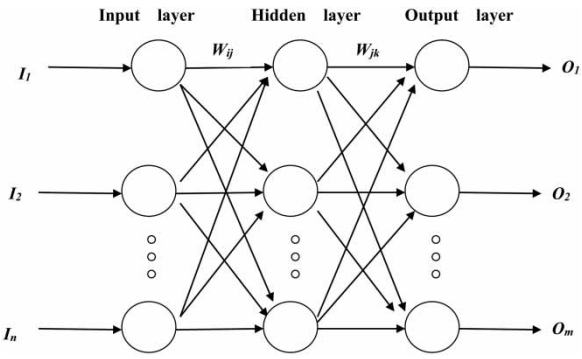

Figure 3 | Three layers of the BP neural network.

chlorinity prediction model. The network consists of the input layer, the hidden or intermediate layers with a non-linear transfer function, and the output layer with a linear transfer function (Sohn *et al.* 1999).

The output of the network O_k can be calculated using the following formula:

$$O_k = \sum_{j=1}^{s} W_{jk} \times F\left(\sum_{i=1}^{n} W_{ij} I_i - \theta_j\right) - \theta_k, \ k = 1, 2, \ \ldots, m, \tag{1}$$

where n, s, and m are the number of neurons in the input layer, hidden layer, and output layer, respectively; W_{ij} is the weight from the input layer to the hidden layer; W_{jk} is the weight from the hidden layer to the output layer; θ_j and θ_k are the threshold values of the hidden layer and the output layer, respectively; I_i is the input for the network, including average daily runoff, low tide, and tidal range in this study, and O_k is the simulated average daily chlorinity; F is the activation function of the hidden layer. In this study, F is a sigmoid function.

The initial weights and thresholds of each neuron can be randomly assigned in the process of training. Simulated values obtained from the model with random weights and target values are then compared. By constantly adjusting the weights and thresholds of each layer, the mean squared error (MSE) of the simulated values from the network model and target values is minimized to the given expectation value.

RESULTS AND DISCUSSION

BP neural network model setup, calibration, and validation

The model was programmed using R. The hyperbolic tangent sigmoid transfer function was used in the hidden layer, whereas a linear transfer function was used in the output layer. A traingdm algorithm was adopted in the training function. The first group data were the input for training and testing; the simulated average daily chlorinity of the Pinggang pumping station obtained from the model and the observed data were compared. The model parameters were constantly adjusted until the MSE between the simulated and the observed data achieved the expected set value. The second group data were the input for validation. The number of training steps for the model was 50,000; the expected training accuracy was 0.05. After multiple rounds of parameter adjustment, the minimized MSE (0.0076) was achieved when the number of hidden layer nodes was 16 and the training step was 13,455.

Comparison between the observed and the simulated estuarine chlorinity from training, testing, and validation results is presented in Figures 4–6. There are good fits between the observed and the simulated estuarine chlorinity in training, testing, and validation periods. That is because the calibration data have better representativeness and the performance of the model in the validation period is

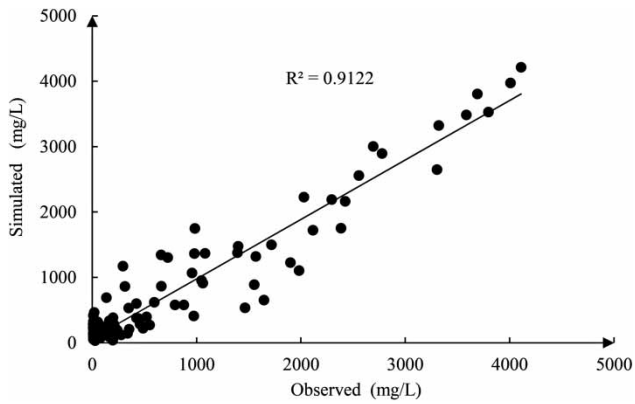

Figure 4 | Comparison between the simulated and observed values of estuarine chlorinity in training period.

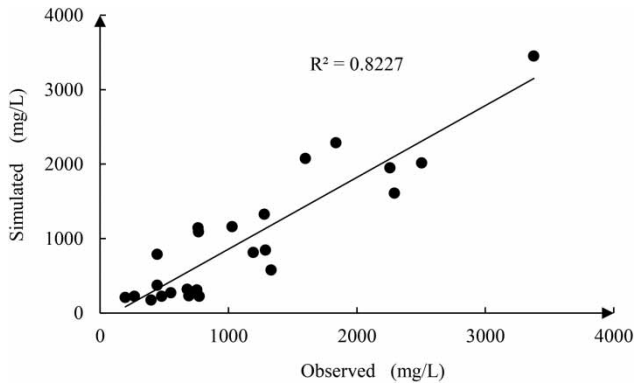

Figure 5 | Comparison between the simulated and observed values of estuarine chlorinity in testing period.

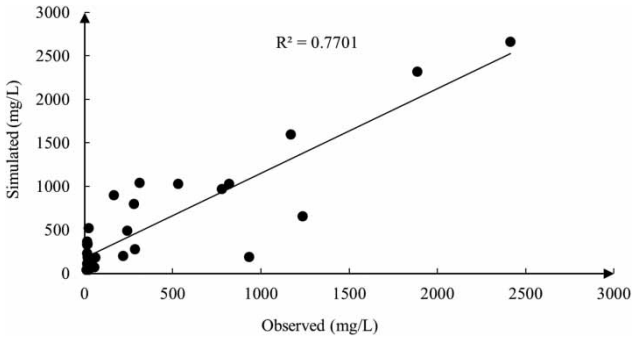

Figure 6 | Comparison between the simulated and observed values of estuarine chlorinity in validation period.

better. Nash–Sutcliffe efficiency (NSE) coefficient and R^2 statistics were used in assessing the BP neural network model training, testing, and validation results. The NSE and R^2 were both 0.91 in the training period, 0.76 and 0.82 in the testing period, and 0.64 and 0.77 in the validation period, respectively, which were acceptable for chlorinity prediction. The BP neural network model can be used to describe changes in the characteristics of estuarine chlorinity. Therefore, according to the runoff and tidal data, the corresponding estuarine chlorinity could be properly simulated using the BP neural network model.

Chlorinity changes under different upstream runoff and boundary conditions of low tide and tidal range

Chlorinity changes under different upstream runoff and nine boundary conditions of low tide and tidal range of the Pinggang pumping station were investigated using the chlorinity prediction model based on the BP neural network (Figure 7). The nine boundary conditions consist of combinations of low tide and tidal range, and both the low tide and tidal range were designed with frequencies of 10%, 50%, and 90%.

Figure 7 shows that, given a certain low tide and tidal range, estuarine chlorinity exhibits a downward trend. This behavior suggests that the larger the upstream runoff, the

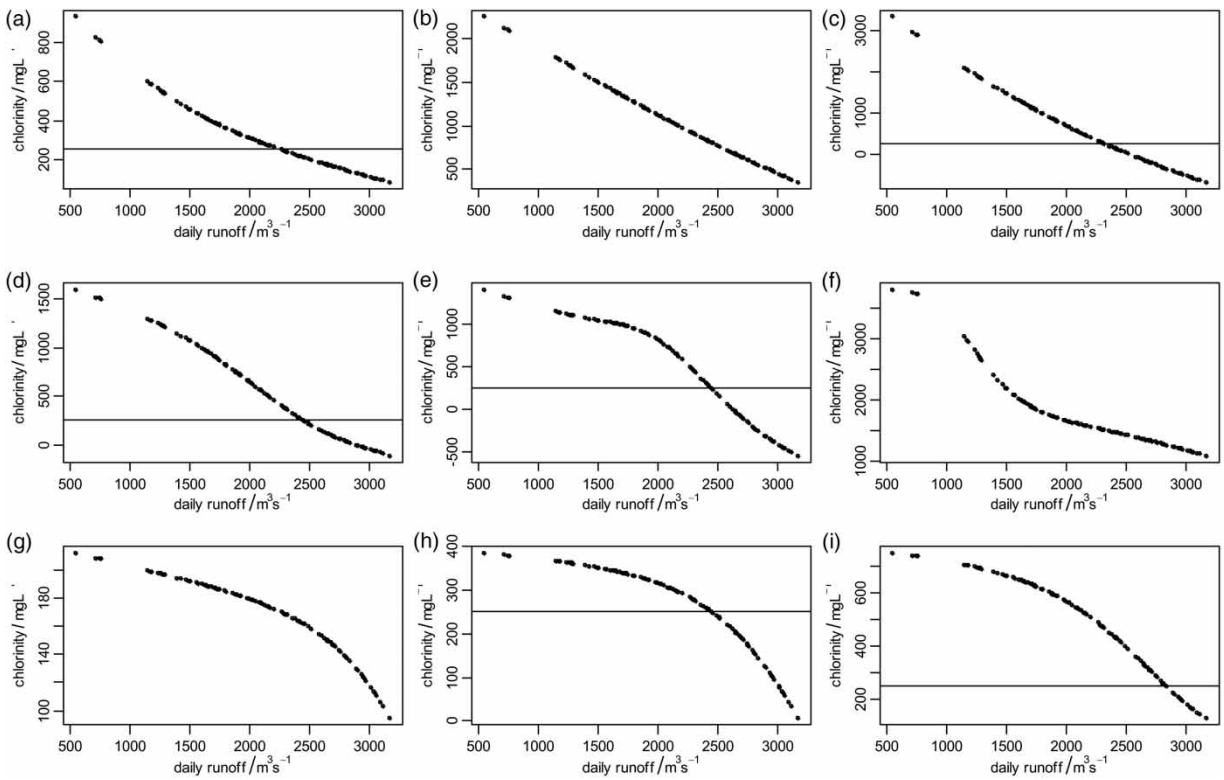

Figure 7 | Chlorinity changes under different daily runoff and frequencies of low tide and tidal range. (a) Low tide: 10%; tide range: 10%. (b) Low tide: 10%; tide range: 50%. (c) Low tide: 10%; tide range: 90%. (d) Low tide: 50%; tide range: 10%. (e) Low tide: 50%; tide range: 50%. (f) Low tide: 50%; tide range: 90%. (g) Low tide: 90%; tide range: 10%. (h) Low tide: 90%; tide range: 50%. (i) Low tide: 90%; tide range: 90%. The black line inside the frame represents the contour line with 250 mg/l chlorinity.

lower the estuarine chlorinity, which is the 'depress salty' effect of the upstream runoff. It also corresponds to the conclusion that water discharge and the tide level downstream are the two most important factors affecting saltwater intrusion in the Qiantang estuary (Han *et al.* 2001). Moreover, Figure 7 also shows that estuarine chlorinity has slightly different changing processes of decline rate under the nine boundary conditions. For example, when the frequency of low tide is 10%, the decline rate of estuarine chlorinity gradually decreases with the increase of upstream runoff; the decline rate first increases and then decreases when the frequency of low tide is 50%; the decline rate gradually increases when the frequency of low tide is 90%. Figure 7 displays the critical upstream runoff for saltwater suppression. We can infer that the range of the critical upstream runoff of the Pinggang pumping station is 2,200–2,800 m^3/s, although the critical upstream runoff relates to low tide and tidal range; it is 2,500 m^3/s in most scenarios. Therefore, it can be concluded that the critical upstream runoff of the Pinggang pumping station is 2,500 m^3/s. It means estuarine chlorinity excessive to the water supply standard occurs with a low probability when the upstream runoff is greater than 2,500 m^3/s.

Figure 7(b) and 7(f) show estuarine chlorinity excessive to the water supply standard occurs within the given range of the upstream runoff, indicating that the effect of the upstream runoff on saltwater suppression is insignificant under the boundary condition of low tide with a frequency of 10% as well as tidal range with a frequency of 50%, or low tide with a frequency of 50% as well as tidal range with a frequency of 90%. Furthermore, Figure 7(g) shows that estuarine chlorinity conforming to the water supply standard occurs under the boundary condition of low tide with a frequency of 90% as well as tidal range with a frequency of 10%, suggesting that, in such a boundary condition, even if an extremely dry year occurs, estuarine chlorinity will still conform to the water supply standard. Given chlorinity changes under different upstream runoff and frequencies of low tide and tidal range, it can be concluded that, when estuarine chlorinity excessive to the water supply standard occurs, averagely, more upstream runoff is required for saltwater suppression under the boundary condition of low tide with a higher frequency. This finding provides a basis for how to regulate the amount of upstream runoff according to real-time tidal level when upstream reservoir discharge is used to depress saltwater intrusion into water sources in the estuarine area. When low tide with a higher frequency (e.g., 90% in the current study) occurs, large amounts of upstream reservoir discharge period by period can effectively alleviate the negative effects on water sources caused by saltwater intrusion, which significantly affects water supply and withdrawals of the estuarine area.

Chlorinity simulation under different frequencies of upstream runoff and tide designs

Eight boundary conditions were designed based on the runoff series of upstream Sanshui and Makou stations for the 1985–2005 period and hourly tidal levels at the Denglongshan station for the 1958–2005 period: the upstream runoff with a frequency of 90% and 97%, low tide and tidal range with a return period of 5 and 10 y. The average daily chlorinity of the Pinggang pumping station under the eight boundary conditions was simulated and calculated with the trained BP neural network model to investigate the changes in the characteristics of estuarine chlorinity under different boundary conditions of upstream runoff and tidal level (Table 1). The simulated result under the aforementioned design was compared with the observed estuarine chlorinity in 2005 to test the performance efficiency of the model. For the upstream runoff with a frequency of 97%, the observed estuarine chlorinity (1,394 mg/L) was similar to the simulated result (1,095 mg/L) under tidal range with a return period of 5 y and the low tide with a return period of 10 y. For the

Table 1 | Simulated estuarine chlorinity under eight boundary conditions obtained from the BP neural network model (mg/L)

	Low tide			
Return period	5 y		10 y	
Upstream runoff frequency	90%	97%	90%	97%
Tidal range				
5 y	618.1	1,415.1	348.4	1,095.4
10 y	1,695.1	2,646.4	328.5	1,197.2

Note: For return periods, 5 and 10 y represent the corresponding tidal range and low tide with return periods of 5 and 10 y.

upstream runoff with a frequency of 90%, the observed estuarine chlorinity (500 mg/L) was similar to the simulated result (618 mg/L) under tidal range with a return period of 5 y and low tide with a return period of 5 y. The comparisons suggest the efficient performance of the model.

Table 1 shows that when the upstream runoff is fixed with a frequency of 90%, the low tide is fixed with a return period of 5 y, the chlorinity of the Pinggang pumping station under the tidal range with a return period of 5 and 10 y were 618.1 and 1,695.1 mg/L, respectively. While when the low daily tide is fixed with a return period of 10 y, the chlorinity of the Pinggang pumping station under the tidal range with a return period of 5 and 10 y were 348.4 and 328.5 mg/L. When an extremely dry year occurs, for example, the upstream runoff is fixed with a frequency of 97%, the chlorinity of the Pinggang pumping station under the tidal range with a return period of 5 y and 10 y were 1,415.1 and 2,646.6 mg/L, respectively, when the low daily tide is fixed with a return period of 5 y. It can be concluded that the higher the designed tidal range and lower daily tides together with the smaller the amount of upstream runoff, the higher the estuarine chlorinity. Liu *et al.* (2014) revealed that the salinity in the Modaomen waterway is largely affected by the tidal range during low-streamflow periods. In the present study, under the same designed tidal level, the average daily chlorinity of the Pinggang pumping station in an extremely dry year (with a frequency of 97%) was, on average, two to four times larger than that in a general year (with a frequency of 90%). Particularly in the extremely dry year, the daily chlorinity of the Pinggang pumping station under the tidal level with a return period of 5 y exceeded 1,400 mg/L, which may seriously reduce the guaranteed rate of water supply in the estuarine area and its surrounding regions. Therefore, during extremely low-flow periods, pumping operations should ensure that freshwater is stored in the backup storage ahead of the tide to prevent serious impacts from saltwater intrusion.

In addition to upstream runoff and tidal range, wind, topography, channel bathometry, interacting downstream branches, and other factors influenced estuarine chlorinity. Saltwater intrusion into the estuary is highly non-linear. For example, closure of the Hongwan and the Hezhou waterways and downstream branches of the Modaomen waterway could decrease saltwater intrusion in the estuary by 20% (Gong *et al.* 2012). Moreover, more saltwater in the Hongwan waterway is spilled over into the Modaomen waterway during neap tides or the coming moderate tide. This occurrence is the inherent dynamic mechanism why saltwater intrusion in the upper Modaomen waterway reaches its maximum during the neap tide or the coming moderate tide (Wang *et al.* 2012). The current study investigated the effect of change in tidal range on estuarine chlorinity by different frequencies of tide designs. However, the dynamic characteristics of saltwater intrusion into the estuary involve complexity and should be further investigated.

CONCLUSION

An estuarine chlorinity prediction model based on the BP neural network for the Modaomen estuary in the PRD, China was constructed, calibrated, and validated using the observed data on upstream runoff, tidal level, and estuarine chlorinity, to investigate the impacts of upstream runoff and tidal level changes on the changing properties of the estuarine chlorinity and obtain the critical upstream runoff for saltwater suppression.

The performance efficiency values of the estuarine chlorinity prediction model were within acceptable margins; the NSE and R^2 in the training period were 0.91 and 0.91, in the testing period were 0.76 and 0.82, and in the validation period were 0.64 and 0.77, respectively. The changing properties of the estuarine chlorinity of the Pinggang pumping station was simulated under nine boundary conditions of low tide and tidal range, suggesting that the decline rate of the estuarine chlorinity varies in each boundary condition when the upstream runoff increases. The critical upstream runoff of the Pinggang pumping station is 2,500 m^3/s for saltwater suppression. The higher the designed tidal range and lower daily tides along with the smaller the amount of upstream runoff, the higher the estuarine chlorinity. In particular, the average daily chlorinity of the Pinggang pumping station in an extremely dry year exceeded 1,400 mg/L under the tidal level with a return period of 5 y. Saltwater intrusion forecasting and upstream reservoir dispatching should be paid attention in the estuarine area in order to prevent or

alleviate negative effects on water supply and withdrawal, especially in dry years.

ACKNOWLEDGEMENTS

The authors would like to express their gratitude to the reviewers for their careful evaluation, as well as pertinent and valuable comments and suggestions, which greatly helped improve the quality of this manuscript. The research is financially supported by National Natural Science Foundation of China (Grant No. 51509127, 91547202, 51479216, and 51569009) and National Key R&D Program of China (2017YFC0405900).

REFERENCES

Abdullah, A. D., Gisen, J. I. A., van der Zaag, P., Savenije, H. H. G., Karim, U. F. A., Masih, I. & Popescu, I. 2016 Predicting the salt water intrusion in the Shatt al-Arab estuary using an analytical approach. *Hydrology and Earth System Sciences* **20**, 4031–4042.

Abdullah, A. D., Popescu, I., van der Zaag, P., Erik, C.-G. M., Karim, U. & Suhail, Q. A. 2018 Optimization of water allocation in the Shatt al-Arab River under different salinity regimes and tide impact. *Hydrological Sciences Journal* **63** (4), 646–656.

Abrahart, R. J., See, L. M. & Dawson, C. W. 2008 Neural network hydroinformatics: maintaining scientific rigour. In: *Practical Hydroinformatics Computational Intelligence and Technological Development in Water Applications* (R. J. Abrahart, L. M. See & D. P. Solomatine, eds). Springer-Verlag, Berlin, Germany, pp. 33–48.

Abrahart, R. J., Anctil, F., Coulibaly, P., Dawson, C. W., Mount, N. J., See, L. M., Shamseldin, A. Y., Solomatine, D. P., Toth, E. & Wilby, R. L. 2012 Two decades of anarchy? Emerging themes and outstanding challenges for neural network river forecasting. *Progress in Physical Geography: Earth and Environment* **36** (4), 480–513.

An, Q., Wu, Y. Q., Taylor, S. & Zhao, B. 2009 Influence of the Three Gorges Project on saltwater intrusion in the Yangtze River Estuary. *Environmental Geology* **56** (8), 1679–1686.

ASCE Task Committee on Application of Artificial Neural Networks in Hydrology 2000 Artificial neural networks in hydrology. I: preliminary concepts. *Journal of Hydrologic Engineering* **5** (2), 115–123.

Bowden, G. J., Maier, H. R. & Dandy, G. C. 2005 Input determination for neural network models in water resources applications. Part 2. Case study: forecasting salinity in a river. *Journal of Hydrology* **301** (1–4), 93–107.

Cheng, X. J., Zhan, W., Guo, Z. R. & Yuan, L. R. 2012 A modeling study on saltwater intrusion to western four watercourses in the Pearl River estuary. *China Ocean Engineering* **26** (4), 575–590.

Colon-Rivera, R. J., Feagin, R. A., West, J. B., Lopez, N. B. & Benitez-Joubert, R. J. 2014 Hydrological modification, saltwater intrusion, and tree water use of a *Pterocarpus officinalis* swamp in Puerto Rico. *Estuarine Coastal and Shelf Science* **147**, 156–167.

Gisen, J. I. A., Savenije, H. H. G., Nijzink, R. C. & Abd Wahab, A. K. 2015 Testing a 1-D analytical salt intrusion model and its predictive equations in Malaysian estuaries. *Hydrological Sciences Journal–Journal Des Sciences Hydrologiques* **60** (1), 156–172.

Gong, W. P., Wang, Y. P. & Jia, J. J. 2012 The effect of interacting downstream branches on saltwater intrusion in the Modaomen Estuary, China. *Journal of Asian Earth Sciences* **45**, 223–238.

Han, Z. C., Pan, C. H., Yu, J. & Chen, H. P. 2001 Effect of large-scale reservoir and river regulation/reclamation on saltwater intrusion in Qiantang Estuary. *Science in China Series B-Chemistry* **44**, 221–229.

He, Y. H., Lin, K. R., Tang, G. P., Chen, X. H., Guo, S. L. & Gui, F. L. 2016 Quantifying the changing properties of climate extremes in Guangdong Province using individual and integrated climate indices. *International Journal of Climatology* **37** (2), 781–792.

Joshi, R., Kumar, K. & Adhikari, V. P. S. 2016 Modelling suspended sediment concentration using artificial neural networks for Gangotri glacier. *Hydrological Processes* **30** (9), 1354–1366.

Ketabchi, H., Mahmoodzadeh, D., Ataie-Ashtiani, B. & Simmons, C. T. 2016 Sea-level rise impacts on seawater intrusion in coastal aquifers: review and integration. *Journal of Hydrology* **535**, 235–255.

Lian, J. J., He, W., Ma, C. & Xu, K. 2015 Guarantee rate of freshwater in a river mouth intruded by saltwater with respect to the joint impact of runoff and tide. *Journal of Hydroinformatics* **17** (6), 917–929.

Liu, D. D., Chen, X. H. & Lou, Z. H. 2010 A model for the optimal allocation of water resources in a saltwater intrusion area: a case study in Pearl River Delta in China. *Water Resource Management* **24**, 63–81.

Liu, B. J., Yan, S. L., Chen, X. H., Lian, Y. Q. & Xin, Y. B. 2014 Wavelet analysis of the dynamic characteristics of saltwater intrusion – A case study in the Pearl River Estuary of China. *Ocean & Coastal Management* **95**, 81–92.

Liu, Z. Y., Chen, X. H., Liu, F., Lin, K. R., He, Y. H. & Cai, H. Y. 2018 Joint dependence between river water temperature, air temperature, and discharge in the Yangtze River: The role of the Three Gorges Dam. *Journal of Geophysical Research: Atmospheres* doi:10.1029/2018JD029078.

Mao, Q. W., Shi, P., Yin, K. D., Gan, J. P. & Qi, Y. Q. 2004 Tides and tidal currents in the Pearl River estuary. *Continental Shelf Research* **24** (16), 1797–1808.

Peirson, W. L., Nittim, R., Chadwick, M. J., Bishop, K. A. & Horton, P. R. 2001 Assessment of changes to saltwater/freshwater habitat from reductions in flow to the Richmond River estuary, Australia. *Water Science and Technology* **43** (9), 89–97.

Rumelhart, D. E., McClelland, J. L. & the PDP Research Group (eds) 1987 *Parallel Distributed Processing: Explorations in the Microstructure of Cognition*. MIT, Cambridge, MA, USA.

Shaha, D. C., Cho, Y. K. & Kim, T. W. 2013 Effects of river discharge and tide driven sea level variation on saltwater intrusion in Sumjin River estuary: an application of finite-volume coastal ocean model. *Journal of Coastal Research* **29** (2), 460–470.

Sohn, S. H., Oh, S. C. & Yeo, Y. K. 1999 Prediction of air pollutants by using an artificial neural network. *Korean Journal of Chemical Engineering* **16** (3), 382–387.

Vijay, R. & Mohapatra, P. K. 2016 Hydrodynamic assessment of coastal aquifer against saltwater intrusion for city water supply of Puri, India. *Environmental Earth Sciences* **75** (7), 588.

Wang, B., Zhu, J. R., Wu, H., Yu, F. J. & Song, X. J. 2012 Dynamics of saltwater intrusion in the Modaomen Waterway of the Pearl River Estuary. *Science China-Earth Sciences* **55** (11), 1901–1918.

Williams, A. A., Lauer, N. T. & Hackney, C. T. 2014 Soil phosphorus dynamics and saltwater intrusion in a Florida estuary. *Wetlands* **34** (3), 535–544.

Xu, K., Zhu, J. R. & Gu, Y. L. 2012 Impact of the eastern water diversion from the south to the north project on the saltwater intrusion in the Changjiang Estuary in China. *Acta Oceanologica Sinica* **31** (3), 47–58.

Yoon, B. I. & Woo, S. B. 2013 Correlation between freshwater discharge and salinity intrusion in the Han River Estuary, South Korea. *Journal of Coastal Research* **2**, 1247–1252.

Yuan, R. & Zhu, J. R. 2015 The effects of dredging on tidal range and saltwater intrusion in the Pearl River estuary. *Journal of Coastal Research* **31** (6), 1357–1362.

Zhang, W., Feng, H. C., Zheng, J. H., Hoitink, A. J. F., van der Vegt, M., Zhu, Y. L. & Cai, H. J. 2013 Numerical simulation and analysis of saltwater intrusion lengths in the Pearl River Delta, China. *Journal of Coastal Research* **29** (2), 372–382.

First received 10 October 2018; accepted in revised form 12 November 2018. Available online 7 December 2018